UCRL- 85977
PREPRINT

CONF-810651--9

Quantitative Measurements Using Soft-X-Ray Streak Cameras

R.L. Kauffman, G.L. Stradling, E.L. Pierce and H. Medecki

This paper was prepared for submittal to the American Physical Society Topical Conference on Low Energy X-Ray Diagnostics held in Monterey, California on June 8-10, 1981.

August, 1981

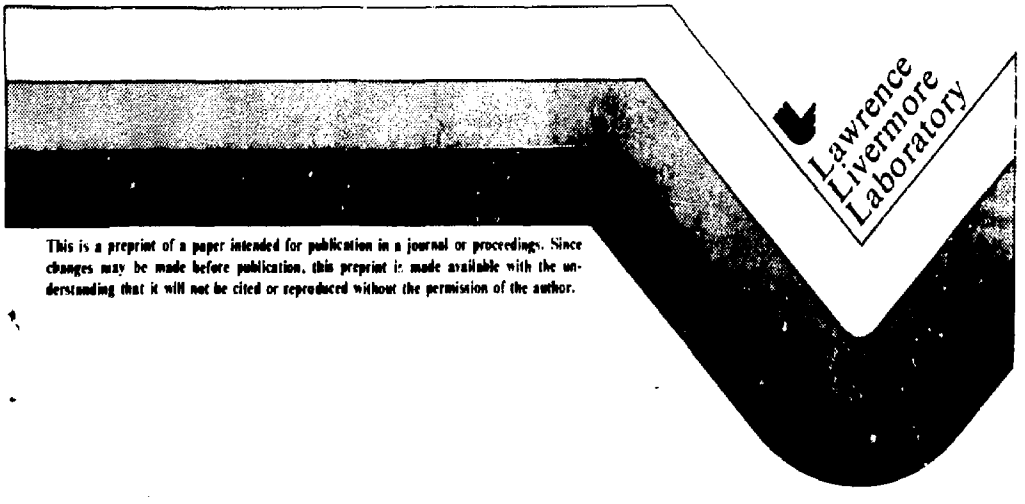

Quantitative Measurements Using Soft-X-Ray Streak Camera*

Robert L. Kauffman, Gary L. Stradling, Edward L. Pierce and Hector Medecki

University of California, Lawrence Livermore National Laboratory, P.O. Box 5508, Livermore, California 94550

ABSTRACT

A Soft X-Ray Streak Camera (SXRSC) is a fast timing instrument sensitive to x rays from 100 eV to 30 keV. The instrument has excellent time resolution (~ 15 ps) and large dynamic range (~ 10^3) which are well suited for measuring x-ray pulses produced by laser-fusion targets. The SXRSC uses a thin transmission photocathode to convert x-rays to a secondary electron signal which is accelerated, focused, and deflected onto a phosphor producing an image of the x-ray pulse time history. In the past, such instruments have been used only to make relative measurements of the time history. At LLNL we have calibrated the SXRSC in order to make absolute intensity measurements of the soft x-ray flux from laser fusion targets. Such measurements will assist in understanding the laser plasma processes and conditions needed to attain laser-produced fusion. Because of the nature of the instrument, we have calibrated it in the dynamic mode using a small laser-produced pulsed x-ray source. Details of the calibrations will be given. We have measured the SXRSC response to be linear over more than two orders of magnitude with the range limited by the x-ray source strength. The dynamic range of similar instruments sensitive to optical light has been demonstrated to be greater than 10^3. Based on first generation calibrations, flux measurements are accurate to ± 30% with the largest uncertainty in the calibrations being in determining the source spectrum and intensity. The uncertainties can possibly be reduced by a factor of two by better source characterization. In that case errors in SXRSC measurements would approach those of other x-ray pulse detectors, such as x-ray diodes.

* Work performed under the auspices of the U.S. Department of Energy by the Lawrence Livermore National Laboratory under Contract No. W-7405-Eng-48.

I. INTRODUCTION

X-ray streak camera technology has been developed at LLNL (1) and elsewhere (2) to time resolve x-ray pulses, primarily for application to laser-fusion plasmas. Such plasmas are intense x-ray sources lasting for nanoseconds or less. At LLNL a soft x-ray streak camera (3) (SXRSC) has been developed which is sensitive to x rays from 100 eV to greater than 30 keV. Its temporal resolution of 15 psec and dynamic range of greater than 10^3 allows for detailed study of the target emission. Until recently, its primary application has been relative time history measurements of the x-ray emission. Efforts have begun to absolutely calibrate the SXRSC for quantitative measurements. In this article some of the SXRSC properties are summarized emphasizing the quantititive calibrations. The calibration method is discussed and some initial results are presented.

II. PRINCIPLE OF OPERATION

The SXRSC operates similarly to optical streak cameras (4) developed at LLNL which is an application of electron imaging technology. Signal processing is illustrated schematically in Fig. 1. First, x rays are converted to an electron signal at the front of the image converter tube. A thin transmission photocathode produces a signal of low-energy secondary electrons at the rear surface whose intensity is proportional to the x-ray intensity striking the front surface. A thin narrow slit ($\sim$ 100 μm wide) collimates the x rays in front of photocathode resulting in secondary electrons being emitted over the slit area. Electrostatic fields accelerate and focus the secondary electrons imaging the slit onto a phosphor at the rear of the image converter tube. The image position at the rear of the tube is controlled by a set of deflection plates in the image converter tube. By rapidly varying the voltage on the deflection plates, the slit image position varies as a function of time resulting in a two-dimensional image on the phosphor.

The temporal history of the x rays is recorded in one dimension orthogonal to the slit while the other dimension is the spatial variation of the x-ray signal along the slit. The light intensity of the phosphor image is amplified with a microchannel plate intensifier (MCP) and recorded either with film or with an active readout CCD array. (5)

An example of x-ray data from a laser fusion target is shown in Fig. 2. The data is recorded with a CCD array using an 8 bit digitizer. In this example several x-ray channels are placed across the slit and their time histories are recorded simultaneously. By combining such data with calibrations discussed below, x-ray flux versus time can be measured.

The SXRSC signal, s, is related quantitatively to the incident x-ray flux, F_x, by the expression

$$s = \frac{d\xi\varepsilon\gamma}{m^2 v_s} \eta F_x \qquad (1)$$

where d is the entrance slit width and v_s is the sweep speed of the deflection plates. The electron transmission efficiency, ξ, image magnification, m, and electron to light conversion efficiency, γ, are properties of the image converter tube and image intensifier. The detection efficiency, η, for either film or CCD array averages over the spectral output of the phosphor. The SXRSC response depends on x-ray energy primarily through the photocathode conversion efficiency, η. Photocathodes normally consist of thin Au films evaporated on carbon substrates although other substrate and cathode materials are being investigated. If the secondary electron spectrum and angular distribution from the photocathode are independent of x-ray energy, the camera parameters, in parenthesis in Eq. (1), are also energy independent. They can be replaced by a single constant, α, characteristic of the instrument and independent of x-ray energy. Eq. (1) then becomes

$$S_x = \alpha \eta_x F_x \quad , \qquad (2)$$

where subscripts denote x-ray energy dependence. Henke et al. (6) have measured of the secondary electron spectrum for various photocathode materials and found them independent of x-ray energy. The energy dependence can also be tested by the energy dependence of the calibrations.

Another application of SXRSC technology is time dependent measurements of x-ray source sizes. By using an x-ray imaging element such as an x-ray microscope (7) or pinhole (8) to image the x-ray source onto the SXRSC slit, the time history of a spatial dimension is recorded. Streaked spectroscopy can also be done by placing the SXRSC slit along the plane of dispersion of a diffraction device such as a crystal (9) or grating. (10)

III. SXRSC PROPERTIES

The unique feature of the SXRSC is its excellent temporal response although its dynamic range, sensitivity, and one dimension of information also make the instrument attractive for pulsed x-ray measurements. Temporal response of the SXRSC is estimated to be 15 psec which is an order of magnitude better than existing x-ray diode-oscilloscope systems. Fig. 3 illustrates the SXRSC temporal response to a series of short x-ray pulses separated by 500 ps. (11) The short x-ray pulses (~ 70 psec) are created by irradiating a Ta foil with a series of 50 psec laser pulses. The pulse shapes are very uniform with little instrumental structure. Temporal data at the 50 psec resolution level can easily be interpreted without complicated instrument response unfolding techniques. The resolution limit of the SXRSC has not been directly measured because a fast, intense x-ray source is not available. Resolution of optical streak cameras having similar design has been demonstrated to be in the sub-10 psec range. (12) Resolution of x-ray streak cameras is expected to be similar. Measured secondary electron distributions from x-ray photocathodes indicate that additional temporal broadening due to the greater energy spread of the secondary electrons

will not decrease temporal resolution significantly. (13) Direct measurements of the temporal response are needed to better understand the instrument response in the 10 psec range.

Spatial resolution is important especially for imaging and spectroscopy applications. Spatial resolution is influenced by broadening in the photocathode and light detection systems as well as by the quality of electron focusing optics. Fig. 4 shows portions of a streaked image from SXRSC in which a 75-μm wire grid is placed in front of the photocathode slit. On the left side of the raw data, the grid is removed displaying the unmodulated pulse. A digital scan along the cathode slit, shown on the right of Fig. 4, displays the 150-μm period indicating that features as small as 7 l.p./mm are clearly resolvable. The noise in the data results from small scale fluctuations in the MCP gain. Signal statistics also contribute to the noise, especially in the wings of the pulse.

Although specific tests have not been made, the dynamic range and sensitivity of the SXRSC are also excellent. From data such as that shown in Fig. 3, no significant broadening is observed at the 50 psec level over three orders of magnitude. A dynamic range of 3×10^3 has been measured with an optical streak camera for 50 psec pulses. (12) The SXRSC also has high sensitivity being determined by the photocathode efficiency. From calibration data minimum detection levels appear to be set by counting statistics due to single photon or electron events in the photocathode. Increased sensitivity can be achieved by widening the slit which enlarges the detection area. Work on optical streak cameras indicate that slits as wide as 1 mm can be used by changing the focus without significantly degrading the temporal resolution. (14) Further studies are needed to assess if the technique is applicable to x-ray streak cameras.

IV. X-RAY PHOTOCATHODE RESPONSE

The useful spectral range of the SXRSC is limited by the x-ray photocathode response. The low energy limit is set by the minimum x-ray

energy transmitted by the photocathode substrate. At high energies, both photocatnode quantum efficiencies and x-ray intensity usually decrease with increasing energy, limiting the useful range to less than about 35 keV. In early development of x-ray streak camera technology, the image converter tubes were sealed requiring a cathode window which could withstand atmospheric pressure. Be windows 8 μm thick limited the useful range of operation to greater than 1 keV. Presently, the SXRSC uses auxiliary pumping equipment allowing for thinner windows which do not have to withstand atmospheric pressure. Present windows of commercially produced vapor-deposited carbon film (15) 50 $\mu g/cm^2$ thick extend the range of sensitivity down to 100 eV. These substrates have proven to be stable under normal operation although they can be destroyed if handled improperly. Thin polymer films are being tested to reduce the lower x-ray limit and to improve detection capability around the carbon K edge which is presently attenuated by the carbon windows. The polymer films should also have improved mechanical strength. Effects of these non-conducting cathode substrate on temporal resolution and dynamic range are presently not known.

Photocathode material, usually Au, is deposited on the substrate window. Its large absorption cross section makes Au an attractive material especially at higher energies. Measurements by Day et al. (16) have shown that its quantum efficiency in the sub-kilovolt region is also high for a metal and relatively stable under normal applications. The photocathode layer must be thick compared to the range of secondary electron contributing to the signal, but relatively thin to minimize absorption in the front region, or dead layer from where secondary electrons cannot escape. Thin film layers also must be thick enough to insure uniform deposition. Henke et al. (17) have found Au thicknesses around 200 A to be optimum. Quantum efficiencies for these transmission photocathodes vary from 0.01 e^-/photon to 0.1 e^-/photon over the range from 100 eV to 10 keV. The Au surfaces are easily prepared by vapor deposition and seem relatively stable when exposed to air. CsI cathodes are also being investigated for increased sensitivity (11). CsI quantum efficiencies are a factor five to thirty greater than

Au quantum efficiencies in the soft x-ray region. (17) Fig. 3 compares the response of CsI and Au photocathodes to the same x-ray pulse train illustrating the increased efficiency. CsI may have a late time temporal component evidenced by the residual signal between pulses in Fig. 3 which may restrict its usefulness. Bateman and Apsimon (18) have also developed a low density CsI cathode which is being employed for x-ray streak camera applications. (19)

V. ABSOLUTE FLUX MEASUREMENT

Absolute flux measurements have begun at LLNL using the SXRSC taking advantage of its excellent timing and large dynamic range. Such measurements require an energy discrimination technique as well as calibration of the instrument. Initial measurements, shown schematically in Fig. 5, use three broad-band channels defined using x-ray mirror-filter pairs. The channels are placed across the SXRSC slit, so that their time histories are recorded simultaneously with a single instrument. For future measurements the number of channels can be expanded by adding more mirror-filter pairs. More precise spectral definition can be obtained using narrow-band interference mirrors, (20) or continuous spectral measurements can be made using a dispersive device such as a transmission grating. (10)

The composition and spectral response of the three initial channels are shown in Fig. 6. These broad-band systems provide energy resolution $\frac{E}{\Delta E} = 3 - 5$, with good channel definition. The transmission filters define a spectral window just below the K or L edge of the filter material. The x-ray mirrors act as low-pass filters having high reflectivity in the spectral window of the filter. At higher energies where the filters become transparent, the mirrors have poor reflectivity suppressing this contribution to the signal.

The transmission filters and mirrors are calibrated individually using auxiliary x-ray sources determining the spectral flux incident on the SXRSC. Below 1 keV the calibrations use a proton-induced line source (21). Results from a Ni mirror calibration is shown in Fig. 7. This

mirror is made by vapor depositing 1000 Å of Ni onto a flat amorphorus carbon substrate. Reflectivity measurements have been extended above 1 keV using an electron bremsstrahlung source from a Ti target. The reflectivity is predicted through the cutoff energy by a semiclassical calculation, (22) while at higher energy the measured reflectivity is less than predicted. At the higher energies x rays are not totally externally reflected at the surface but penetrate through the Ni layer to the carbon substrate. Lower reflectivity from the low Z carbon substrate produces an observed reflectivity less than predicted for bulk Ni. Use of higher Z films on a low Z substrate appears viable for improving the low pass filter qualities of x-ray mirrors. Improved computational capabilities now being developed for x-ray interference mirrors should be useful in predicting their reflectivities.

VI. SXRSC CALIBRATIONS

SXRSC calibrations are done in the pulsed, or dynamic, mode using the broad-band channels defined above. Such calibrations are necessary because late time background signals can interfere with a steady-state, or d.c., calibrations. The background is easily suppressed electronically in pulsed operation. Other transient field effects may also affect d.c. calibration. For pulsed calibration, x-ray sources on the order of 10^{18} photons/cm^2-sec are required. These photon fluxes are at least three orders of magnitude greater than obtainable from a d.c. source but can be readily obtained from a pulsed x-ray source.

Present calibrations use laser-produced x-ray pulses. A schematic of the calibrations is shown in Fig. 8. Laser pulses of around one joule and 50 psec are focused at normal incidence onto targets of various material. Three calibrated x-ray diodes (XRD) monitor the source at 45^0 to the target plane. The SXRSC views the target at 45^0 on the opposite to the XRD's as shown in Fig. 8. The SXRSC is calibrated for the three x-ray channels described in the flux measurements. The channel response of the three XRD's have been matched as nearly as possible to

the SXRSC channel responses. The SXRSC response, R_{SXRSC}, is related to the signal ratio from the two instruments as shown in Fig. 8. The signal ratio is corrected for the difference in effective width of the two corresponding energy channels and for the difference in solid angle of the two instruments. The XRD response, R_{XRD}, is the channel response averaged over the input spectrum. The R_{SXRSC} is similarly averaged by the input spectrum.

The laser source spectrum is structured depending on target material with most of its energy contained below 1 keV for these irradiation conditions. Spectral intensities for several targets measured by the XRD's is shown in the top curve of Fig. 9, and total conversion efficiency from incident laser energy to x-ray output in this spectral region is plotted in the bottom curve. While precise values depend on irradiation conditions, the high Z elements of Ta and Au produce a more intense x-ray source over this energy region. For lower Z elements, line emission effects are more evident. For example, the intensities from Fe and V targets are similar at 200 eV and 400 eV, but at 600 eV the V intensity is an order of magnitude larger, approaching that of Ta and Au. In this region V L-shell emission dominates the spectrum. Preliminary high resolution measurements in this region, shown in Fig. 10, display the complicated spectrum produced by these targets. The spectra in Fig. 10 are taken using an Fe filter which cuts off the spectrum at 710 eV, although the line structure extends to higher energies. By suitably mating the filter and target material, high intensity emission in a relative narrow band region may be possible.

SXRSC calibration data is similar to that shown in Fig. 2. Intensity vs. time curves for the three x-ray channels are integrated in time and compared with the integral signal from the XRD's. An example of the comparison for the 600 eV channel is shown in Fig. 11. Similar data is obtained for the two lower energy channels. The XRD output has been converted to absolute fluences at the SXRSC, correcting for its solid angle and channel width. The SXRSC signal unit, bit, is an arbitrary value set by the CCD digitizer which is constant for the particular instrument.

The calibration value determined by the slope of the data in Fig. 11 varies with target Z. The high Z, high intensity data are systematically above the lower Z data. These systematics are due to broad-band responses used for energy discrimination and to structure in the source spectrum. Even by including these systematics, the data group about a mean value shown as the solid line in Fig. 11 with an error of ± 20%. The total errors in the flux measurements are estimated to be ± 30% when errors in the auxiliary calibrations are included.

Similar calibrations have been done on another SXRSC using Kodak Royal X-Pan film as a detector. The calibration data are from Argus, a larger, experimental laser. The data are from several experiments accumulated over a number of months. The integrated SXRSC signal from each of the three x-ray channels is plotted in Fig. 12 versus the x-ray fluence from the same spectral region measured by a ten channel XRD system. (23) Each film record uses a stepwedge registered on the film with a constant, chromatically matched, light source, to relate a given optical density to a light exposure. This procedure approximately corrects for shot to shot variations in film developing and film response. The mean calibration value, shown as solid lines in Fig. 12, relate the incident x-ray flux to the light intensity, or exposure. The dashed lines in Fig. 12 represent the statistical errors of the data which in this case are about ± 18%. The calibrations are linear over a dynamic range of two orders of magnitude. The lower limit of the dynamic range is limited by the sensitivity of the instrument. The upper limit is set by target output from this shot series. Data from other experiments have shown linearity over at least another order of magnitude.

During the experiments several different photocathodes have been used. All are 300 Å of Au vapor deposited on 50-$\mu g/cm^2$ thick carbon foils. No systematic variations between different cathodes are observed. Sensitivity appears stable over several months and is reproducible within the errors of the measurements.

The calibrations can be used to infer the SXRSC instrument response. The mean energy and width of the three channels are listed in

Table I along with average photocathode response, $\overline{R\eta}$. The average photocathode response is calculated by averaging quantum efficiencies measured by Henke et al. (17) over the x-ray channel assuming a flat spectrum. Using these values the instrument response, α, is obtained from the total channel response in Fig. 12 and is listed in Table I. The results relate film intensity to electron current density from the photocathode and are given in the final column in Table I. The values are constant for the three channels within $\pm$ 25% as would be expected if the photocathode secondary electron spectrum and angular dependence are independent of energy as discussed in Section IV. The calibrations can be extrapolated to other x-ray channels using these values without requiring each channel to be calibrated independently.

The instrument's sensitivity can be deduced from the instrument response. For a channel 1 mm wide and with 15-psec time resolution the minimum measurable intensity is about 20 for a 100 μm wide slit. For α = 0.022 this corresponds to a current density of 900 e^-/cm^2-ps from that area which translates into about 13 e^- from the photocathode. This lower limit approaches the limit set by electron statistics from these Au cathodes. Sensitivities can be increased by using CsI cathodes which have quantum efficiencies around one. Cathode sensitivities greater than one would not increase the instrument sensitivity because photon statistics would then limit the minimum detection level.

VII. QUANTITATIVE ANALYSIS

The calibration values in the previous section can be used to reduce relative time history data to average flux. As an example the raw data from a representative Argus shot are analyzed, and resulting absolute flux values for the three energies are shown in Fig. 13. The data is from an Au disk irradiated with 35 joules of 0.53 μm light with a 680 ps pulse. These can be summed appropriately to obtain total x-ray flux from the target. Such data can help understand the complicated

process of laser absorption and energy transport in laser-fusion targets. By coupling the instrument with better resolution devices quantitative detailed spectral studies can be made.

VIII. CONCLUSIONS

The SXRSC is an instrument which has demonstrated fast-timing characteristics, good dynamic range and high sensitivity making it useful for measuring fast x-ray pulses such as those from laser-fusion targets. Efforts have begun to absolutely calibrate the instrument to make a quantitative measurement. Measurements accurate to $\pm$ 30% are possible using the initial calibration scheme. The accuracy is limited by the use of broad band channels and x-ray diodes to monitor the source spectra. Higher resolution measurements of the target spectrum may allow the spectral dependence to be unfolded from the data. Narrower channel definition would also improve calibrations. By using x-ray interference mirrors to define a narrow band of x rays, the dependence on the x-ray spectrum would decrease. A more powerful calibration source is needed to implement such a scheme. These improvements could improve calibrations so that SXRSC accuracies could approach XRD measurements. More accurate flux monitoring detectors are needed for further improvement of the calibrations. For a more accurate measurement, d.c. calibrations should be explored. Present state-of-the-art in quantitative SXRSC measurements can still prove valuable for pulsed x-ray flux measurements and energy balance experiments.

IX. ACKNOWLEDGMENTS

We would like to thank Burt Henke for his support in photocathode development and for supplying us with CsI photocathodes. We would like to acknowledge Stan Thomas for electronics support of the SXRSC effort and Jack Cheng, Jack Noonan and Gary Tripp for the active readout CCD arrays. We thank Jerry Gaines, Dick Ernst, and Earl Augusta for support

of the auxiliary calibrations. We acknowledge Claude Dittmore for help in film detection techniques. We also acknowledge David Gaines and Ray Perkins for their spectroscopy effort at the monojoule and Julia Kanakanui for the SXRSC resolution analysis.

REFERENCES

1. C.F. McConaghy and L.W. Coleman, Appl. Phys. Lett. 25, 268 (1974); L. Coleman and D. Attwood, Laser Program Annual Report - 1974, edited by J.I. Davis (Lawrence Livermore Laboratory, Livermore, CA, UCRL-50021-74, 1974) pp. 315-319.
2. For a recent review of streak camera technology see Proceedings of the 13th International Conference on High Speed Photography and Photonics, edited by Shin-ichi Hyodo (Japanese Society of Precision Engineering, Tokyo, Japan, 1979).
3. G.L. Stradling, M. S. Thesis, Brigham Young University, 1981; Lawrence Livermore National Laboratory, UCRL-52568.
4. S.W. Thomas, G.R. Tripp and L.W. Coleman, Proceedings of the 10th International Congress on High Speed Photography, edited by E. Laviron (Association Nationale de la Recherche Technique, Paris, France, 1972) pp. 127-133; S. Thomas, J. Houghton, T. Owen and L. Coleman, Laser Program Annual Report - 1974 edited by J.I. Davis (Lawrence Livermore Laboratory, Livermore, CA, UCRL-50021-74, 1974) pp. 292-296.
5. J. Cheng, G. Tripp, and L. Coleman, International Conference on the Application of CCD devices (San Diego, CA, 1978).
6. B.L. Henke, J.A. Smith, and D.T. Attwood, J. Appl. Phys. 48, 1842 (1977).
7. R.H. Price, Laser Program Annual Report Vol. 2, edited by L. Coleman (Lawrence Livermore National Laboratory, Livermore, CA UCRL-50021-79, 1979) pp. 5-54 to 5-57; and "X-Ray Microscopy Using Reflection Optics" presented at this conference.
8. D.T. Attwood, L.W. Coleman, M.J. Boyle, J.T. Larsen, D.W. Phillion, and K.R. Manes, Phys. Rev. Lett. 38, 282 (1977).
9. M.H. Key, C.L.S. Lewis, J.G. Lunney, A. Moore, J.M. Ward, and R.K. Thareja, Phys. Rev. Lett. 44, 1669 (1980).
10. N.M. Ceglio, M. Roth, and A.M. Hawryluk, this conference.
11. G.L. Stradling, H. Medecki, R.L. Kauffman, D.T. Attwood, and B.L. Henke, Appl. Phys. Lett. 37, 782 (1980).

12. S.W. Thomas and G.E. Phillips, Proceedings of the 13th International Conference on High Speed Photography and Photonics, edited by Shin-ichi Hyodo (Japanese Society of Precision Engineering, Tokyo, Japan, 1979) 471.

13. B.L. Henke and K. Premaratne, Proceedings of the International Conference on X-Ray and XUV Spectroscopy, Jpn. J. Appl. Phys. 17 suppl. 17-2 pp. 477-482 (1978).

14. R.A. Lerche, H. Medecki, G.E. Phillips, and S.W. Thomas, IEEE Conference on Plasma Science, 1981, 1113; Lawrence Livermore National Laboratory UCRL-86019, 1981.

15. Arizona Carbon Foil Co., Tuscon, AZ

16. R.H. Day, P. Lee, E.B. Salomon and D.J. Nagel, LA-UR-79-1360, IEEE International Conference on Plasma Science, Montreal, Quebec, Canada, June 1979.

17. B.L. Henke, J.P. Knauer, and K. Premaratne, J. Appl. Phys. 52, 1509 (1981).

18. J.E. Bateman and R.J. Apsimon, unpublished.

19. M.H. Key and J.E. Bateman, Rutherford Laboratory Report, RL-79-036 (1979).

20. G.L. Stradling, T.W. Barbee, Jr., B.L. Henke, E.M. Campbell, and W.C. Mead, presented at this conference.

21. R.W. Kuckuck, J.L. Gaines and R.D. Ernst, Proceedings of the 4th Conference of Scientific and Industrical Applications of Small Accelerators, edited by J. Duggan and I.L. Morgan, (IEEE, Piscataway, NJ, 1976) 229.

22. A. Toor, private communications.

23. K.G. Tirsell, H.N. Kornblum, and V.W. Slivinsky, Bull. Amer. Phys. Soc. 23, 807 (1978); Lawrence Livermore National Laboratory UCRL-81478 (1979).

TABLE I

ANALYSIS OF THE THREE CHANNEL RESPONSES

$\overline{E}$ (eV)	ΔE (eV)	$\overline{R\eta}$ (e^-/keV) x 10^{-3}	$\left(\frac{\overline{R\eta}\,\Delta E\alpha}{\text{Int. - psec}}{\text{J/keV - cm}^2}\right)$ x 10^{10}	$\left(\frac{\alpha \text{ Int}}{e^-/cm^2 - psec}\right)$
210	79	6.48	8.8 ±2.2	0.028 ±0.002
395	254	2.82	10.1 ± 2.5	0.022 ± .002
600	234	7.20	19.1 ± 3.7	0.018 ± .002

Fig. 1 Schematic showing signal processing for an x-ray streak camera.

Fig. 2 Example of SXRSC data. Top is the two dimensional image of the intensity vs time recorded by a CCD array. Bottom is the time history of three subkilovolt x-ray energies defined by filter material labeled on each curve.

Fig. 3 Example of the temporal response of the SXRSC to 70 psec x-ray pulses separated by 500 psec for Au and CsI photocathodes.

Fig. 4 SXRSC response to 150 μm period modulations across the entrance slit. On the left is the raw data while on the right is a digital scan of the data across the slit.

Fig. 5 Schematic of spectral flux measurements using SXRSC. X-ray mirror-filter pairs define three subkilovolt x-ray channels along the slit of the SXRSC.

Fig. 6 Spectral response of the three SXRSC channels used for the flux measurements.

Fig. 7 Example of the x-ray mirror calibrations. The sub-kilovolt data is taken using a proton-induced line source. Above 1 keV, an electron bremsstrahlung source is used.

Fig. 8 Schematic of the absolute calibrations. The SXRSC signals are compared with signals from calibrated XRD's.

Fig. 9 X-ray yields from the laser-produced source measured using XRD's. The top curves show the spectral dependence of various targets while the lower curve shows the Z dependence of the total x-ray yield in the energy region.

Fig. 10 High resolution measurements illustrating the complicated structure from some targets in this energy region.

Fig. 11 Calibration data for SXRSC. Systematics in the data indicate dependence on input spectra although all data cluster around a mean value shown as a solid line.

Fig. 12 Calibration curves for the three x-ray channels. The solid circles (●) are from Au targets irradiated using 2 ω_0 (λ = 0.53 μm) light and open circles (○) using 3 ω_0 (λ = 0.26 μm) light. Some Ti (▲, △) and Be (■, □) data are also plotted.

Fig. 13 Spectral fluxes from a typical shot derived using calibration values in Fig. 12. The x-ray pulse is from an Au disc irradiated with 35J, 680 ps pulse at 2 ω_0 laser light.

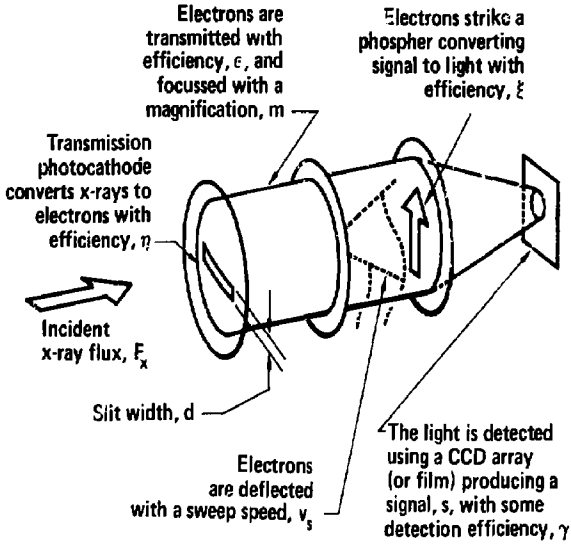
Electrons are transmitted with efficiency, ε, and focussed with a magnification, m
Electrons strike a phospher converting signal to light with efficiency, ξ
Transmission photocathode converts x-rays to electrons with efficiency, η
Incident x-ray flux, F_x
Slit width, d
Electrons are deflected with a sweep speed, v_s
The light is detected using a CCD array (or film) producing a signal, s, with some detection efficiency, γ

Fig. 1

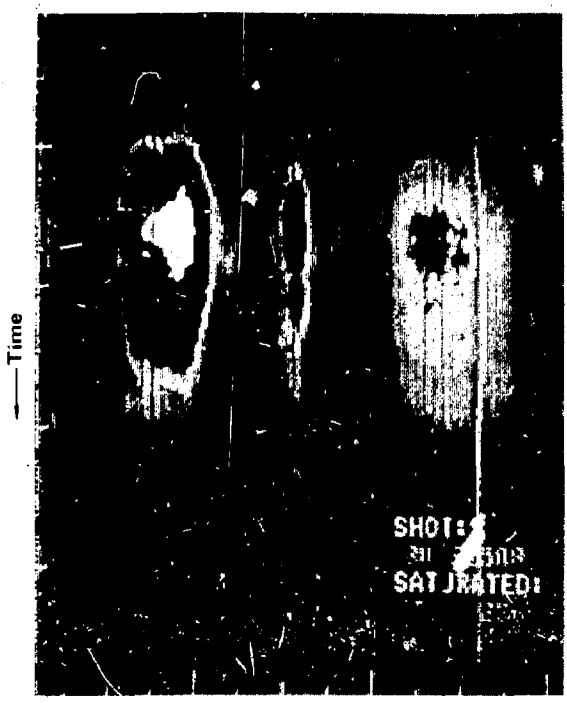

Shot #80121508
E_L = 3.90 kJ, τ_L = 900 ps
$I_{max} \sim 3 \times 10^{15}$ W/cm^2

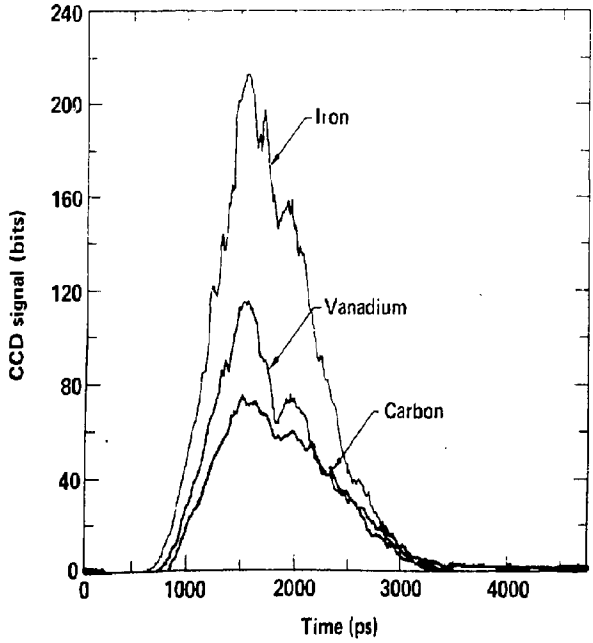

Fig. 2

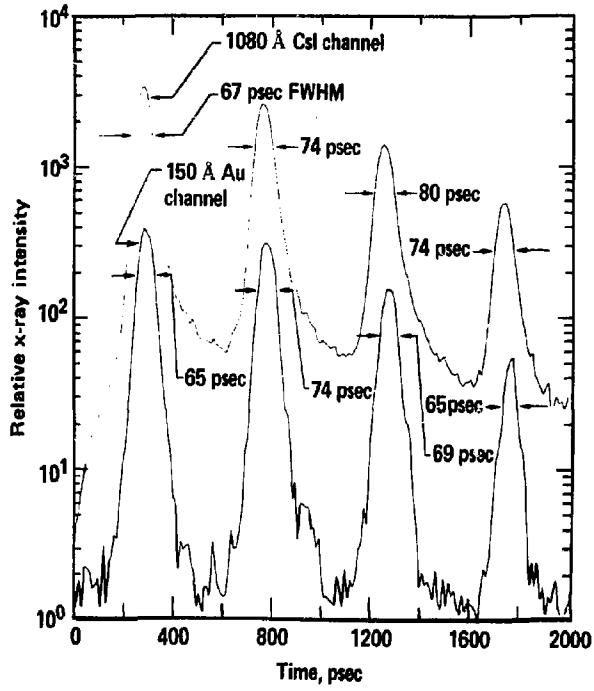
1080 Å CsI channel
67 psec FWHM
74 psec
150 Å Au
channel
80 psec
74 psec
65 psec
74 psec
65psec
69 psec
Relative x-ray intensity
Time, psec
10^4
10^3
10^2
10^1
10^0
0
400
800
1200
1600
2000

Fig. 3

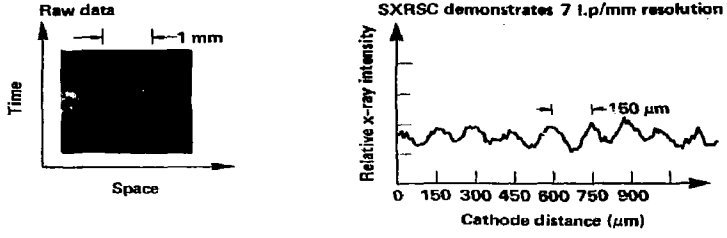
Raw data
1 mm
Time
Space
SXRSC demonstrates 7 l.p/mm resolution
Relative x-ray intensity
150 μm
0 150 300 450 600 750 900
Cathode distance (μm)

Fig. 4

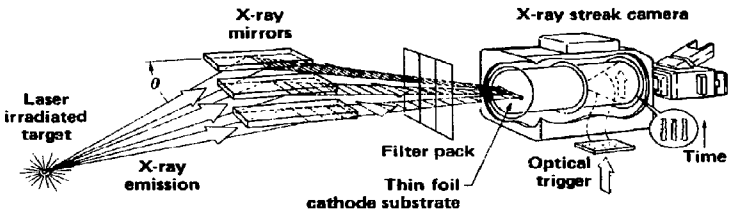
X-ray
mirrors
X-ray streak camera
θ
Laser
irradiated
target
X-ray
emission
Filter pack
Thin foil
cathode substrate
Optical
trigger
Time

Fig. 5

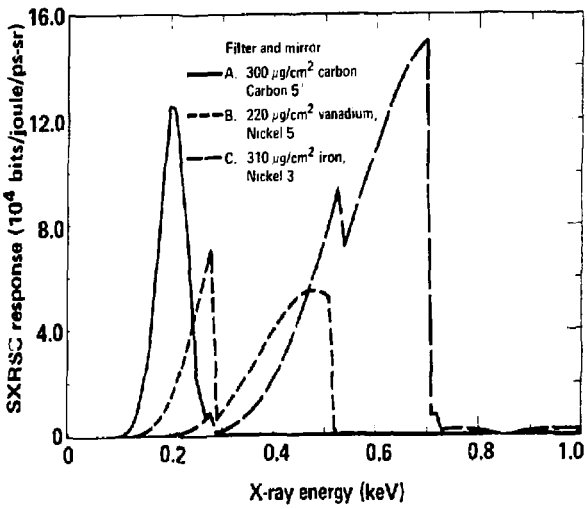
Filter and mirror
A. 300 μg/cm² carbon
Carbon 5
B. 220 μg/cm² vanadium,
Nickel 5
C. 310 μg/cm² iron,
Nickel 3
SXRSC response (10⁴ bits/joule/ps-sr)
16.0
12.0
8.0
4.0
0
0
0.2
0.4
0.6
0.8
1.0
X-ray energy (keV)

Fig. 6

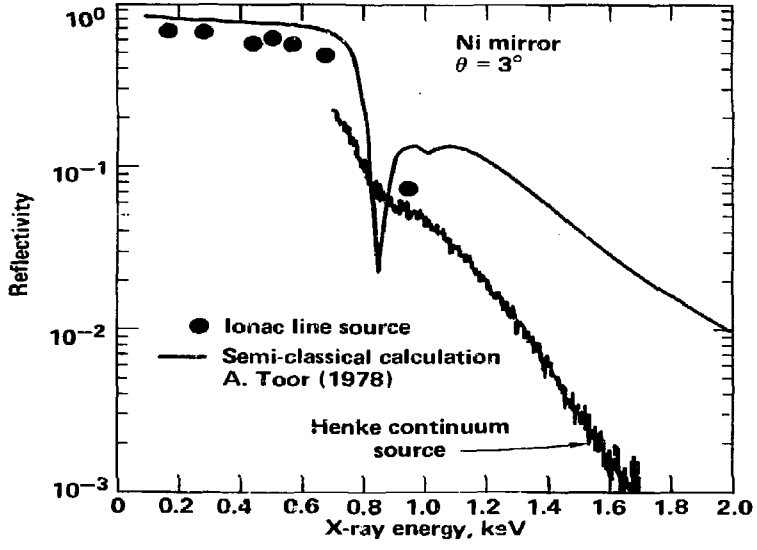
Ni mirror
θ = 3°
Ionac line source
Semi-classical calculation
A. Toor (1978)
Henke continuum
source
Reflectivity
X-ray energy, keV
10^0
10^-1
10^-2
10^-3
0
0.2
0.4
0.6
0.8
1.0
1.2
1.4
1.6
1.8
2.0

Fig. 7

A schematic of the calibrations

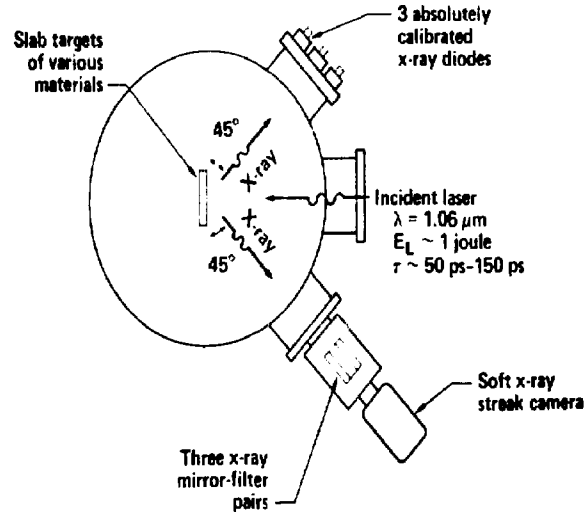

$$R_{SXRSC} = R_{XRD} \frac{\Omega_{XRD}}{\Omega_{SXRSC}} \frac{\Delta E_{XRD}}{\Delta E_{SXRSC}} \frac{S_{SXRSC}}{S_{XRD}}$$

The SXRSC calibrations

- Are done in the dynamic mode using 70-170 ps x-ray pulses
- Use a broad band x-ray source with $h\nu < 1$ keV
- Use transmission filters to define three coarse x-ray channels
- Are done by comparing x-ray fluences measured by calibrated x-ray diodes (XRD's) to the integral signal from the SXRSC

Fig. 8

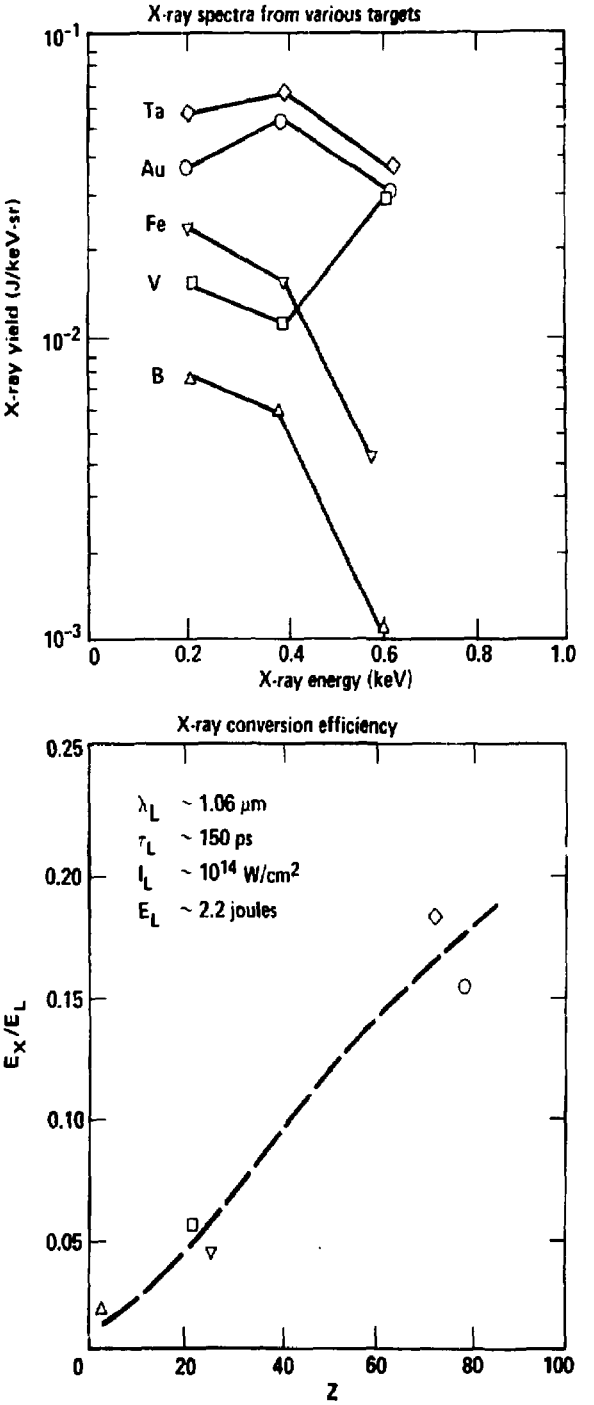
X-ray spectra from various targets
X-ray yield (J/keV-sr)
10^{-1}
10^{-2}
10^{-3}
Ta
Au
Fe
V
B
0
0.2
0.4
0.6
0.8
1.0
X-ray energy (keV)
X-ray conversion efficiency
E_X/E_L
0.25
0.20
0.15
0.10
0.05
λ_L ~ 1.06 μm
τ_L ~ 150 ps
I_L ~ 10^{14} W/cm^2
E_L ~ 2.2 joules
0
20
40
60
80
100
Z

Fig. 9

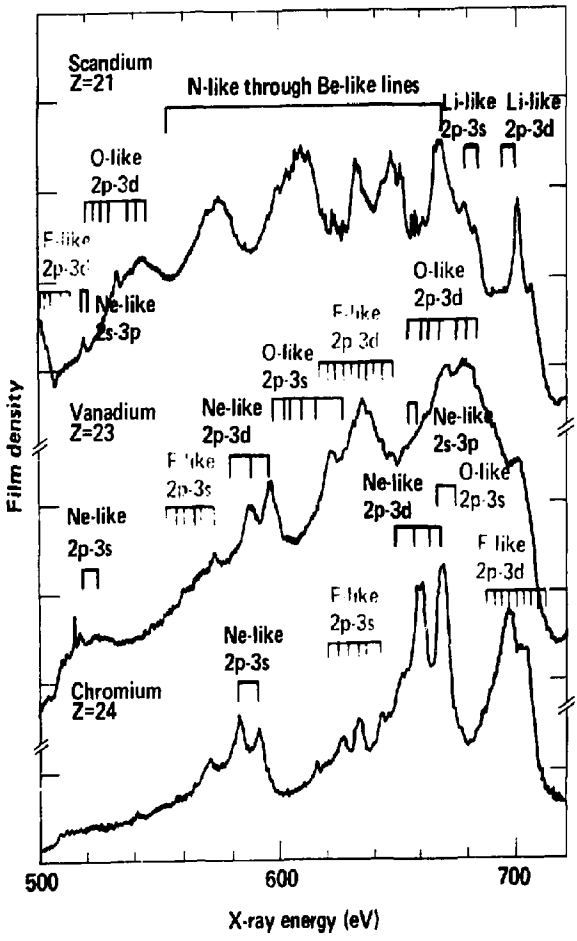
Scandium
Z=21
N-like through Be-like lines
Li-like
2p-3s
Li-like
2p-3d
O-like
2p-3d
F-like
2p-3d
Ne-like
2s-3p
O-like
2p-3d
F-like
2p-3d
O-like
2p-3s
Vanadium
Z=23
Ne-like
2p-3d
Ne-like
2s-3p
F-like
2p-3s
Ne-like
2p-3d
O-like
2p-3s
Ne-like
2p-3s
F-like
2p-3d
F-like
2p-3s
Ne-like
2p-3s
Chromium
Z=24
Film density
500
600
700
X-ray energy (eV)

Fig. 10

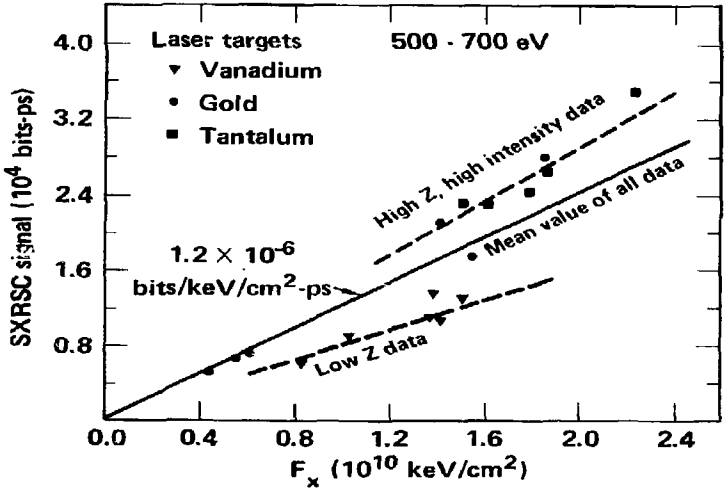
Laser targets
Vanadium
Gold
Tantalum
500 - 700 eV
High Z, high intensity data
Mean value of all data
Low Z data
1.2 × 10⁻⁶
bits/keV/cm²-ps
SXRSC signal (10⁴ bits-ps)
4.0
3.2
2.4
1.6
0.8
0.0
0.4
0.8
1.2
1.6
2.0
2.4
F_x (10¹⁰ keV/cm²)

Fig. 11

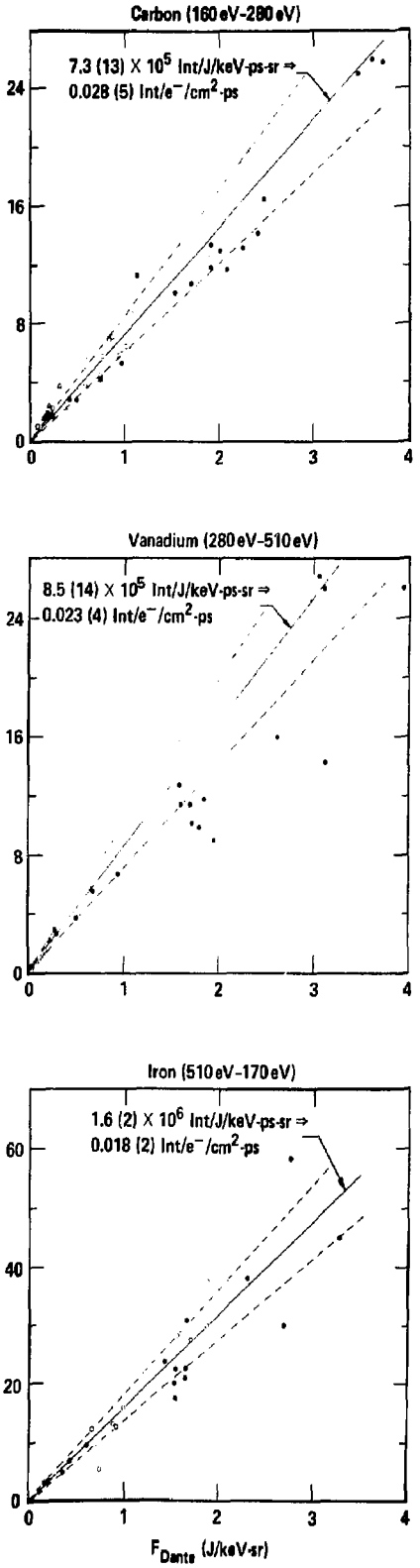
Carbon (160 eV-280 eV)
7.3 (13) X 10^5 Int/J/keV-ps-sr ⇒
0.028 (5) Int/e⁻/cm²-ps
Vanadium (280 eV-510 eV)
8.5 (14) X 10^5 Int/J/keV-ps-sr ⇒
0.023 (4) Int/e⁻/cm²-ps
Iron (510 eV-170 eV)
1.6 (2) X 10^6 Int/J/keV-ps-sr ⇒
0.018 (2) Int/e⁻/cm²-ps
F_Dante (J/keV-sr)

Fig. 12

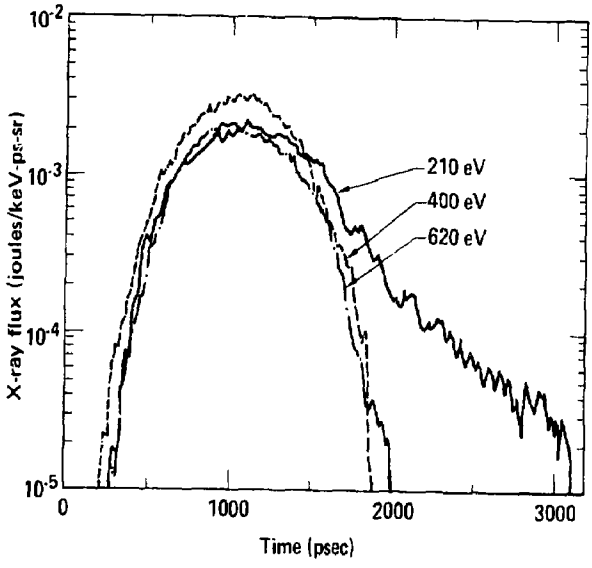
10^{-2}
10^{-3}
10^{-4}
10^{-5}
X-ray flux (joules/keV-ps-sr)
210 eV
400 eV
620 eV
0
1000
2000
3000
Time (psec)

Fig. 13